UHASSELT
KNOWLEDGE IN ACTION

Maastricht University

Faculty of Medicine and Life Sciences
School for Life Sciences
Master of Biomedical Sciences

Master's thesis

The good, the fat, the ugly: Elongation of long-chain fatty acids in control of lesion progression and repair in multiple sclerosis

Elke Smeets

Thesis presented in fulfillment of the requirements for the degree of Master of Biomedical Sciences, specialization Molecular Mechanisms in Health and Disease

SUPERVISOR :
dr. Sanne VERBERK
Prof. dr. Jerome HENDRIKS

MENTOR :
Mevrouw Tine WEYTJENS

2023
2024

Transnational University Limburg is a unique collaboration of two universities in two countries: the University of Hasselt and Maastricht University.

UHASSELT
KNOWLEDGE IN ACTION

www.uhasselt.be
Universiteit Hasselt
Campus Hasselt:
Martelarenlaan 42 | 3500 Hasselt
Campus Diepenbeek:
Agoralaan Gebouw D | 3590 Diepenbeek

UHASSELT
KNOWLEDGE IN ACTION

Maastricht University

Faculty of Medicine and Life Sciences
School for Life Sciences
Master of Biomedical Sciences

Master's thesis

The good, the fat, the ugly: Elongation of long-chain fatty acids in control of lesion progression and repair in multiple sclerosis

Elke Smeets

Thesis presented in fulfillment of the requirements for the degree of Master of Biomedical Sciences, specialization Molecular Mechanisms in Health and Disease

SUPERVISOR :

dr. Sanne VERBERK

Prof. dr. Jerome HENDRIKS

MENTOR :

Mevrouw Tine WEYTJENS

The good, the fat, the ugly: Elongation of long-chain fatty acids in control of lesion progression and repair in multiple sclerosis

Elke Smeets[1], Tine Weytjens[2], Sanne Verberk[2] and Jerome Hendriks[2]

[1]Department of Medicine and Life Sciences, University Hasselt, Campus Diepenbeek, Agoralaan Building D 3590 Diepenbeek, Belgium.
[2]Department of Immunology and Infection, Biomedical Research Institute (BIOMED), Hasselt University, Agoralaan Gebouw C 3590 Diepenbeek, Belgium.

*Running title: *Role of fatty acid elongation in demyelination*

To whom correspondence should be addressed: Jerome Hendriks, Tel: +32 (11) 26 92 07; Email: Jerome.Hendriks@uhasselt.be

Keywords: Multiple sclerosis, Macrophage, Fatty acid metabolism, Remyelination, Inflammation

ABSTRACT

Multiple sclerosis (MS) stands out as one of the most prevalent demyelinating diseases of the central nervous system (CNS), for which no effective cure exists. A main hallmark of MS is the formation of demyelinating lesions in which infiltrated macrophages and CNS-resident microglia accumulate. While these phagocytes can exhibit neuroprotective features by clearing myelin debris, prolonged accumulation of myelin-derived lipids shifts them toward a disease-aggravating state. The underlying pathways governing this phenotypic shift in MS remain inadequately understood. Our recent findings have pinpointed disrupted fatty acid synthesis as a fundamental player in these phenotypic alterations. Specifically, the transcriptional levels of elongation of very long chain fatty acids proteins (Elovl)1 were significantly reduced after acute myelin exposure in macrophages. Therefore, this study aimed to elucidate the role of ELOVL1 in shaping the phagocyte phenotype in MS. Here, we show that inhibition of ELOVL1 alters the inflammatory and metabolic characteristics of macrophages. Specifically, we observed a reduced lipid load and increased abundance of lipid efflux transporter ABCA1 in myelin-loaded macrophages. In addition, ELOVL1 suppression and inflammatory activation altered the expression of *Elovl2, 5, 6* and *7* in macrophages. Moreover, ELOVL1 inhibition appeared to promote remyelination in an *ex vivo* brain slice culture. These findings indicate that ELOVL1 inhibition in phagocytes may potentially be an effective strategy to promote remyelination in demyelinating disorders such as MS.

Abbreviations: ABCA1: ATP Binding Cassette subfamily A member 1, ABCG1: ATP Binding Cassette subfamily G member 1, ARG1: Arginase 1, BMDM: Bone marrow-derived macrophage, BSC: Brain slice culture, CNS: Central nervous system, CNTF: Ciliary neurotrophic factor, ELOVL: Elongation of very long-chain fatty acids proteins, FA: Fatty acid, HMDM: Human monocyte-derived macrophage, IGF1: Insulin growth factor 1, IL: Interleukin, LCFA: Long-chain fatty acid, LD: Lipid droplet, LPS: Lipopolysaccharide, LRP1: Low-density lipoprotein receptor-related protein 1, MBP: Myelin basic protein, MFI: Mean/Median fluorescent intensity, MS: Multiple sclerosis, MUFA: Mono-unsaturated fatty acid, NF: Neurofilament, NGF: Nerve growth factor, NO: Nitric oxide, NOS2: Nitric oxide synthase 2, OL: Oligodendrocyte, OPC: Oligodendrocyte precursor cell, ORO: Oil Red O, PPAR: Peroxisome proliferator-activated receptor, PUFA: Poly-unsaturated fatty acid, SCD1: Stearoyl-CoA desaturase-1, SFA: Saturated fatty acid, TGFβ1: Tumor growth factor β1, TNFα: Tumor necrosis factor α, VLCFA: Very long-chain fatty acid.

INTRODUCTION

Multiple sclerosis (MS) is a chronic demyelinating autoimmune disease of the central nervous system (CNS), affecting 2.8 million people globally (1, 2). MS stands out as the most prevalent cause of non-traumatic disability in young adults and predominately afflicts women (2, 3). This devastating disease is marked by demyelinated lesions appearing in both the white and grey matter (4-6). These arise from dysregulated immune responses, resulting in the destruction of the protective myelin sheaths surrounding the axons (4). Until now, the etiology of the disease remains still unclear. However, it is suggested that the disease onset is induced by a confluence of genetic predisposition and various environmental stimuli such as viral infections and lifestyle factors (2, 7). In the early stages of MS, demyelination triggers the activation of endogenous repair mechanisms, facilitating the restoration of myelin sheaths of demyelinated axons through remyelination (5). Oligodendrocytes (OLs), maturing from oligodendrocyte precursor cells (OPCs), play a pivotal role in generating these newly formed myelin sheaths (8-10). However, remyelination is limited since OPCs fail to differentiate into OLs as the disorder advances (9, 11). Clinical manifestations of MS include a variety of physical, neurological, and cognitive impairments such as forgetfulness, fatigue, and muscle spasms, drastically compromising the patient's quality of life (12). Available disease-modifying therapies delay disease progression and limit symptoms in early disease stages, yet fall short in halting cognitive and neurologic decline as the disease progresses (3, 5). Therefore, there is an urgent need for novel therapies that are not only effective in the initial disease phase but also in the chronic progressive stage when endogenous repair mechanisms frequently fail, and neurodegeneration prevails.

A main pathological hallmark of MS is the accumulation of infiltrated macrophages and CNS-resident microglia in the demyelinating lesions (4). Initially, these phagocytes were predominantly perceived as contributors to the development of MS lesions, promoting demyelination and neuroinflammation through the release of inflammatory and toxic mediators (13, 14). However, recent insights have unveiled the highly dynamic nature of the phagocyte phenotype, enabling them to transition from a pro-inflammatory, disease-promoting state to a disease-resolving phenotype in MS (15, 16). These protective phagocytes actively clear lipid-rich myelin debris within the lesions while concurrently secreting anti-inflammatory and neurotrophic factors (15-17). These reparative functions are crucial for facilitating the remyelination of damaged myelin sheaths. While ingestion of myelin-derived lipids initially induces a reparative phenotype in phagocytes, excessive myelin accumulation eventually diminishes their protective characteristics, reverting them to a disease-promoting phenotype (18, 19). The underlying pathways governing this phenotype switch in MS remain inadequately understood.

Our research group discovered that disturbed fatty acid (FA) metabolism underlies these phenotypic changes of macrophages and microglia in demyelinating conditions (19, 20). FA species that are endogenously synthesized or ingested through our diet can be further desaturated and elongated by members of the FA desaturase and elongase families (Fig. 1) (21, 22). Growing evidence suggests a close association between the activity of these enzymes and the inflammatory and metabolic characteristics of phagocytes (23-25). Our recent findings have revealed that stearoyl-CoA desaturase-1 (SCD1), an enzyme involved in FA desaturation, triggers an inflammatory phenotypic shift of phagocytes following sustained exposure to myelin. This shift occurred due to impaired lipid efflux, resulting in intracellular accumulation of myelin-derived lipids. Notably, SCD1 inhibition restored the efflux ability of phagocytes, preventing inflammatory phenotypic shift and promoting remyelination in both *ex vivo* and *in vivo* MS models (19). Furthermore, our research group revealed the involvement of FA elongation in shaping the phagocyte phenotype (20). Elongation of very long-chain fatty acids proteins (ELOVLs), also referred to as elongases, are FA elongation enzymes located in the endoplasmatic reticulum. ELOVLs extend the carbon chain of FAs, forming both long-chain (LCFAs) and very long-chain FAs (VLCFAs). These FAs are important for the synthesis of various lipid molecules, such as triglycerides and phospholipids. Additionally, VLCFAs are also crucial for maintaining neuronal membrane integrity and facilitating myelination (26, 27). In

mammals, seven elongases (ELOVL1-7) have been identified, each exhibiting its substrate specificity. ELOVL1, 3, 6 and 7 are selective for saturated (SFAs) and mono-unsaturated FA (MUFAs) while ELOVL2, 4 and 5 elongate polyunsaturated FA (PUFAs) (21, 26). In terms of expression, *Elovl1*, *Elovl5,* and *Elovl6* are expressed ubiquitously while *Elovl2*, *Elovl3*, *Elovl4*, and *Elovl7* exhibit a tissue-specific expression pattern (21). Our research group has shown that the expression of *Elovl6*, responsible for elongating C16 SFAs and MUFAs, was markedly elevated in macrophages after sustained myelin exposure (20). Furthermore, phagocyte-specific deficiency of ELOVL6 induced a reparative phenotype, stimulating remyelination in both *ex vivo* and *in vivo* MS models (20). These findings have highlighted the involvement of FA metabolism in shaping the phagocyte phenotype, underscoring its therapeutic implications in MS.

Interestingly, the expression of *Elovl1*, the elongase that follows *Elovl6* by elongating C18, C20, C22, and C24 SFAs, diminishes in macrophages after acute myelin exposure (20). ELOVL1 has already been shown to be involved in the pathology of X-linked adrenoleukodystrophy (X-ALD), a demyelinating disease that involves the toxic accumulation of VLCFAs, especially C26:0 FAs, in plasma and tissues (28). Furthermore, the accumulation of saturated VLCFAs has been linked to a pro-inflammatory phenotype in macrophages (29). This indicates that ELOVL1 could present an interesting target to drive the phagocyte phenotype. Nevertheless, the impact of ELOVL1 on phagocyte function and remyelination in the context of MS remains to be elucidated.

Therefore, this study aimed to elucidate the role of ELOVL1 in shaping the phagocyte phenotype in MS. We hypothesize that modulating FA metabolism by inhibition of ELOVL1 can skew phagocytes to a disease-resolving phenotype, stimulating remyelination in MS. Our study demonstrated that the ELOVL1 suppression modulates the inflammatory and metabolic features of macrophages. Additionally, ELOVL1 inhibition was found to influence the transcriptional levels of other *Elovl*s in inflammatory macrophages. Furthermore, ELOVL1 inhibition seemed to facilitate remyelination in an *ex vivo* brain slice demyelination model. Overall, our findings show that ELOVL1 influences the phagocyte phenotype, highlighting its potential therapeutic relevance in demyelinating disorders such as MS.

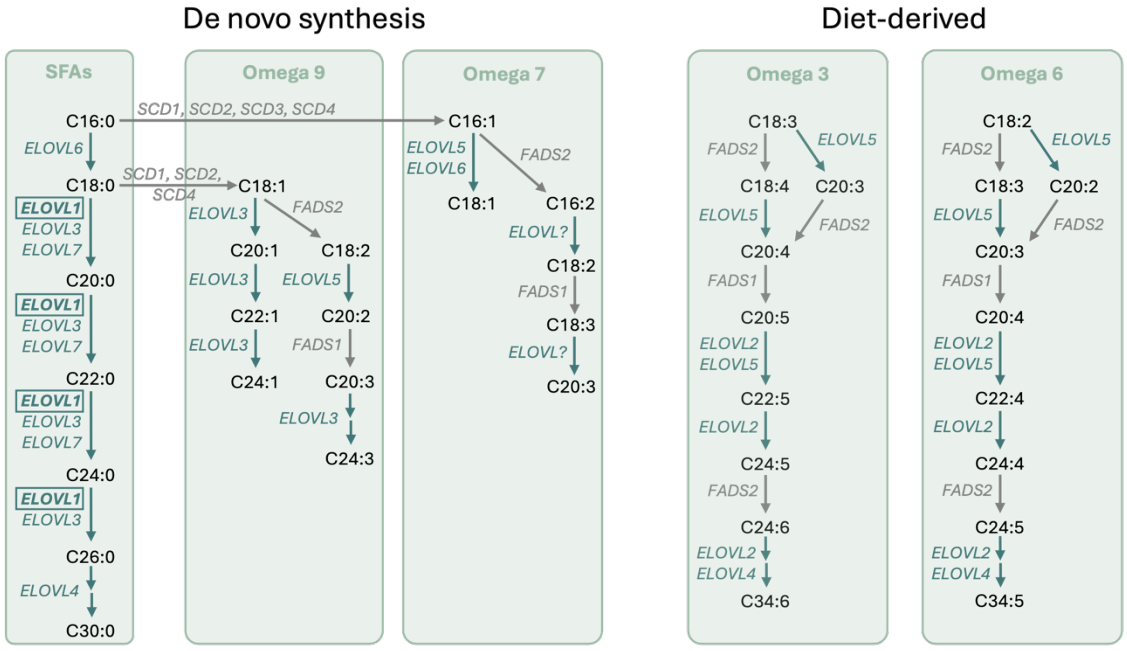

Fig. 1 – Biosynthesis of long-chain and very long-chain fatty acids (FAs). Starting from palmitic acid (C16:0), saturated FAs and unsaturated FAs of omega 7 and omega 9 series can be synthetized by various elongation (green arrows) and desaturation (grey arrows) steps. Additionally, unsaturated FAs of omega 3 and omega 6 series are synthetized by precursor C18:2 and C18:3 FAs that are obtained from the diet. Figure modified from (21).

EXPERIMENTAL PROCEDURES

Animals – Wild-type C57BL/6J mice were purchased from Envigo. Mice were housed on a 12 h light/dark cycle with *ad libitum* access to water and a standard chow diet. All animal procedures were conducted in accordance with the institutional guidelines and approved by the Ethical Committee for Animal Experiments of Hasselt University.

Cell isolation and culture – Mouse bone marrow-derived macrophages (BMDMs) were obtained as previously described (30). Briefly, macrophages were isolated from femoral and tibial bone marrow of 10-12-week-old female mice and cultured in RPMI 1640 medium supplemented with 15% L929-conditioned medium (LCM, in-house production as described by Weischenfeldt *et al.* (31)), 10% fetal calf serum (FCS), and 0.5% penicillin/streptomycin. Cultures were maintained at 37°C in an atmosphere of 5% CO_2 and 95% relative humidity for 7 days. Fresh medium was added on day 4. Afterward, BMDMs were collected using PBS/EDTA (10 mM) and plated at 0.5×10^6 cells/ml in the described culture medium containing 5% LCM. In addition, human monocyte-derived macrophages (HMDMs) of healthy controls were isolated and cultured as described by Bogie *et al.* (19, 30). Primary mouse OPCs were isolated and cultured as described before (32, 33). The detailed explanation can be found in Supplementary Materials and Methods. All reagents used are listed in Table S1.

Myelin isolation and stimulation – Myelin was isolated from post-mortem mouse and human brain tissue through density gradient centrifugation, as described previously (34). The BCA protein assay kit was used to measure the protein concentration, according to the manufacturer's instructions. BMDMs and HMDMs were treated daily with mouse (100 µg/ml) and human (10 µg/ml) myelin, respectively, for 24 h (acute) or 72 h (sustained) or left untreated.

Pharmacological treatments and macrophage stimulation – BMDMs and cerebellar brain slices were pre-treated with 4 or 8 µM ELOVL1 inhibitor (ELOVL1-22 in 99% ethanol solution, 10 mg/ml) or vehicle (ethanol, 0.01%) for 30 min, followed by incubation with myelin. Cells undergoing ELOVL1 inhibitor treatment for 24 h were treated once, while those treated for 72 h received the treatment every 24 h. For pro- and anti-inflammatory phenotyping, cells were stimulated with lipopolysaccharide (LPS, 100 ng/ml) or interleukin 4 (IL4, 20 ng/ml), respectively.

Cerebellar brain slice culture (BSC) – Cerebellar slices were isolated and cultured as described previously (35, 36). The detailed explanation can be found in Supplementary Materials and Methods. Demyelination was induced with lysolecithin (0.5 mg/ml) for 18 h. After demyelination and one day of rest, slices were treated daily with ELOVL1 inhibitor or vehicle for 7 days, followed by histological analysis.

RNA extraction and quantitative PCR – BMDMs were lysed using QIAzol. Total RNA was extracted using the RNeasy mini kit. Concentration and quality were measured using the NanoDrop ND-1000 spectrophotometer (Thermo Fisher Scientific). Complementary DNA was synthesized using the qScript™ cDNA SuperMix, according to the manufacturer's instructions. Real-time quantitative PCR was conducted on a Step One Plus detection system (Applied Biosystems, Gaasbeek, Belgium). The reaction was conducted for 5 min at 25°C, 30 min at 42°C, and 5 min at 85°C using T100 PCR Thermal Cycler (BioRad). Quantitative PCR was conducted on a StepOnePlus™ real-time PCR system (Applied Biosystems). The PCR reaction mixture contained SYBR green master mix, 10 µM of forward and reverse primers, nuclease-free water, and 12.5 ng template cDNA were added in a total reaction volume of 10 µL. Data was analyzed using the comparative Ct method and normalized to CycA, Tbp and Hprt. Primer sequences are depicted in Table S2.

Phagocytosis assay – The ability and extent of myelin phagocytosis was assessed using myelin fluorescently labeled with 1,19-dioctadecyl-3,3,39,39-tetramethylindocarbocyanine perchlorate (DiI). BMDMs were treated with DiI-myelin (100 µg/ml) for 1.5 h. The fluorescence intensity was measured by the LSRFortessa Flow Cytometer (BD Biosciences) and analysis was performed with FlowJo v10.10 CellQuest Software (Treestar).

Nitric oxide (NO) determination and arginase activity assay – Release of NO was determined in culture supernatants of treated BMDMs stimulated with LPS for 18 h using Griess reagent system (2.5% H_3PO_4, 1% sulfanilamide, and 0.1%

N-(1-Naphthyl) ethylenediamine dihydrochloride). Optical density was measured with the CLARIOstar PLUS microplate reader (BMG Labtech) at 540 nm. Arginase activity was defined on cell lysates using 0.1% Triton X-100, 25 mM Tris-HCl (pH 7.5) and 1x protease inhibitor cocktail. Arginase was activated by adding 3.5 µL of 10 mM $MnCl_2$ to 10 µL sample at 56°C for 10 min. Next, samples were incubated with 0.5 M L-arginine (pH 9.7) for 60 min at 37°C. The reaction was stopped by adding 90 µL stop solution (96% H_2SO_4/85% H_3PO_4/H_2O 1:3:7) and incubated with α-isonitrosopropiophenone (9%) for 30 min at 95°C. Samples were left in the dark to cool down to room temperature (RT) until measurement of optical density at 540 nm. Enzymatic activity was calculated by the following equation: [Urea] × (total volume × 10^6) / (tested volume × Time(incubated at 37°C) × 1000).

Oil red O (ORO) staining – BMDMs were cultured on glass cover slides and fixed in 4% paraformaldehyde (PFA) for 15 min. To stain intracellular neutral lipids, BMDMs were incubated with 0.3% ORO for 10 min at RT. After the slides were washed with tap water, cells were counterstained with hematoxylin for 30 s and rinsed in running tap water for 5 min. Analysis was performed with Leica DM2000 LED microscope (Leica Microsystems, Wetzlar, Germany) and Fiji (ImageJ, version 2.14.0) software.

Flow cytometry – Single-cell suspensions were blocked with 10% goat serum and subsequently stained with anti-ABCA1 primary antibody for 45 min at 4°C. This was followed by incubation with the suitable secondary antibody for 45 min at 4°C. An unstained and secondary antibody-only control was taken into account. To evaluate cellular viability, cells were treated with 7AAD. Lipid content assessment was conducted by staining cells with BODIPY for 15 min at 37°C. Unstained cells were used as a negative control. The LSRFortessa Flow Cytometer was used to quantify cellular fluorescence, and the median or mean fluorescence intensity (MFI) was adjusted for background MFI in FlowJo. All antibodies are depicted in Table S3.

Immunofluorescence microscopy and image analysis – PFA fixed BMDMs on glass slides were permeabilized with 0.1% Triton X-100 in PBS for 1 min at RT. Blocking was performed using 10% Dako protein block in PBS for 1 h at RT. Slides were incubated with anti-ABCA1 and nuclei were stained using 4,6′-diamidino-2-phenylindole (DAPI). Analysis was performed with Leica DM4000 B microscope (Leica Microsystems, Wetzlar, Germany) and Fiji software. PFA fixed cerebellar slices were blocked with blocking buffer (1x PBS + 5% horse serum + 0.3% Triton X-100). Subsequently, slices were incubated at 4°C overnight with anti-MBP and anti-NF antibodies diluted in blocking buffer. Next, slices were incubated with the appropriate secondary antibodies for 1 h at RT. Images were acquired using an LSM900 Airyscan 2 Confocal microscope (Zeiss, Zaventem, Belgium) and analyzed using Fiji software.

Immunoblotting – BMDMs were lysed with radioimmunoprecipitation assay buffer (150 mM NaCl, 50 mM Tris, 1% SDS, 1% Triton X-100, 0.5% sodium deoxycholate) containing protease inhibitor. Protein concentrations of the cell lysates were determined using a BCA Protein Assay kit. Samples were separated on an SDS-polyacrylamide gel (12% resolving gel, 4% stacking gel) by electrophoresis and transferred onto a polyvinylidene fluoride membrane. Subsequently, membranes were blocked with 5% dried skimmed milk powder in PBS with 0.1% Tween-20 for 1 h, followed by overnight incubation with anti-ELOVL1 antibody at 4°C. Next, the membrane was incubated for 1 h with appropriate full HRP-conjugated secondary antibody. The Amersham Imager 680 (GE Healthcare Life Sciences) was used to detect chemiluminescent signals, using the enhanced chemiluminescence Plus detection kit. Densitometry analysis was performed using ImageJ and normalized to Cy5 using the QuickStain Protein labeling kit.

Statistical analysis – Data were statistically analyzed using GraphPad Prism V9 (La Jolla, CA, USA) and visualized as mean ± standard deviation (SD). The Shapiro-Wilk test was utilized to test for normal distribution. Normally distributed data was analyzed by a two-tailed unpaired Student's t-test (with Welch's correction if necessary) or an ANOVA (Tukey's post hoc analysis). For non-normally distributed data, Kruskal-Wallis or Mann-Whitney analysis was applied. P values <0.05 are considered statistically significant (*, $P < 0.05$; **, $P < 0.01$; ***, $P < 0.001$; ****, $P < 0.0001$).

RESULTS

Acute myelin exposure diminishes both gene expression and protein abundance of ELOVL1 in murine BMDMs – Recently, our research group has revealed that myelin internalization alters the gene expression of *Elovls* in phagocytes (20). Specifically, acute myelin exposure resulted in a reduction in *Elovl1* gene expression in macrophages (20). To investigate whether myelin uptake alters the protein abundance of ELOVL1 in phagocytes in the same manner, murine BMDMs were treated with myelin for acute (24 h) and sustained (72 h) periods, indicative of a reparative and inflammatory macrophage phenotype, respectively (19, 37). Protein expression was determined in cell lysates by western blot (Fig. S1). Following acute myelin exposure, we observed a trend toward a decreased ELOVL1 protein abundance in BMDMs (Fig. 2A). Consistent with our findings at the gene level (20), prolonged exposure to myelin resulted in an ELOVL1 abundance comparable to the levels observed without myelin stimulation (Fig. 2A). To determine if these alterations are also evident for human ELOVL1, HMDMs were treated with human myelin. Remarkably, acute myelin exposure resulted in an upward trend of ELOVL1 protein abundance compared to unstimulated cells (Fig. 2B). In addition, sustained exposure to myelin caused a decreased abundance compared to acute exposure (Fig. 2B). These results suggest that myelin internalization alters ELOVL1 abundance in both murine and human macrophages; however, in a species-specific manner.

Pharmacological inhibition of ELOVL1 slightly alters the inflammatory phenotype of macrophages – Recent studies state that phagocytes contribute to remyelination through clearing damaged myelin and producing neurotrophic factors (37, 38). However, metabolic dysfunction caused by excessive lipid accumulation hinders their reparative features (19). To investigate the role of ELOVL1 in determining the inflammatory and metabolic macrophage phenotype, we utilized an established ELOVL1 inhibitor (39). This compound has been shown to reduce C24:0 and C26:0 synthesis levels (IC_{50} = 0.0004 µM in human HEK293 cells), consistent with the inhibition of ELOVL1, and is specific for ELOVL1 over ELOVL6 and ELOVL7, for which it has minimal activity (IC_{50} values > 50 µM for ELOVL6 and 7 in human HEK293 cells) (39). Pharmacological inhibition of ELOVL1 (4 and 8 µM) in BMDMs did not impact cell viability, as studied with a 7AAD viability staining (Fig. S2). Notably, exposure to myelin slightly decreased the percentage of live cells. A control without ethanol was included since this solvent was used for the ELOVL1 inhibitor

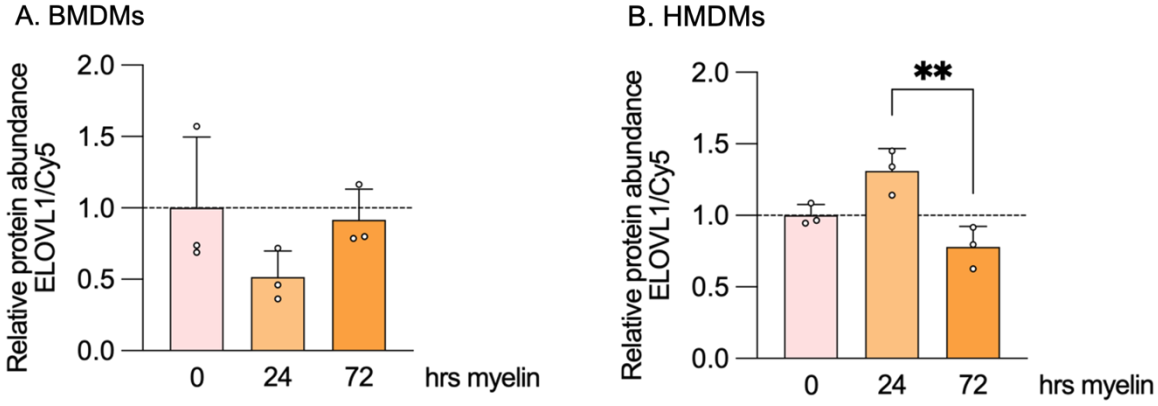

Fig. 2 – Murine macrophages showed a trend toward a reduced ELOVL1 protein abundance after acute myelin exposure, a change not observed in human macrophages. (A, B) Quantified protein ELOVL1 abundance after western blot analysis of (A) murine bone marrow-derived macrophages (BMDMs) and (B) human monocyte-derived macrophages (HMDMs) that were left untreated (0 h) or treated with acute (24 h) or sustained exposure (72 h) to 100 µg/ml murine and 10 µg/ml human myelin, respectively (n = 3 wells, for HMDMs: 3 persons). ELOVL1 protein abundance was normalized for total protein abundance by Cy5 staining. Data are represented as mean ± SD. **, P < 0.01; one-way ANOVA.

and served as the vehicle, demonstrating that ethanol itself did not influence viability (Fig. S2). To elucidate whether ELOVL1 inhibition impacts the inflammatory phenotype of macrophages, we examined the gene expression of inflammatory mediators in BMDMs. To this end, BMDMs were first pre-treated with 8 μM of ELOVL1 inhibitor or vehicle for 30 min and were subsequently treated with myelin for 24 h or left untreated. Considering that phagocytes encounter an inflammatory environment in MS lesions (18), the cells were subjected to the prototypical inflammatory stimulus LPS. Interestingly, ELOVL1 inhibition in the absence and presence of myelin stimulation did not alter the expression of the inflammatory genes in unstimulated cells (Fig. 3A-D). Following LPS induction, ELOVL1 inhibition reduced the *Il1b* expression and enhanced the *Nos2* expression in BMDMs without myelin compared to the vehicle (Fig. 3A, C). Moreover, myelin exposure decreased the expression of all inflammatory genes in LPS-stimulated cells compared to those that were not exposed to myelin (Fig. 3A-D), consistent with previous findings demonstrating that acute myelin exposure results in less inflammatory macrophage features (15, 16). Next, we investigated the gene expression of arginase 1 (*Arg1*) and neurotrophic factors in BMDMs treated with 8 μM of ELOVL1 inhibitor or vehicle for 24 h, followed by IL4 stimulation. Even though IL4 enhanced *Arg1* expression, its levels were unchanged after ELOVL1 inhibition with and without stimulation (Fig. 3E). In addition, ELOVL1 inhibition did not result in alterations in neurotrophic factors (Fig. 3F). Furthermore, we performed an NO and arginase assay in BMDMs treated with 8 μM of ELOVL1 inhibitor or vehicle and myelin for 24 h or 72 h to estimate L-arginine metabolism assay via NOS2/arginase (40). The arginase activity diminished after ELOVL1 inhibition with acute ($P = 0.0931$) and sustained myelin exposure but remained unchanged in the absence of myelin (Fig. 3G). In addition, ELOVL1 suppression did not alter NO_2^- levels in LPS-stimulated macrophages (Fig. 3H). These results suggest that ELOVL1 is a possible important mediator of the inflammatory status of macrophages.

ELOVL1 inhibition impacts the metabolic phenotype of macrophages – Since the ELOVL1 expression is altered in myelin-stimulated macrophages, we examined whether ELOVL1 inhibition impacts the metabolic phenotype of macrophages. Therefore, we evaluated the uptake, intracellular processing, and efflux of myelin-derived lipids by BMDMs. ORO and BODIPY were used to stain neutral lipids, which are predominantly found in lipid droplets (LDs) (41). ORO staining showed a reduction in lipid load in BMDMs treated with ELOVL1 inhibitor and myelin for 72 h compared to the vehicle (Fig. 4A, B). Additionally, a downward trend in the number of LDs per cell was observed following 24 h ELOVL1 inhibitor and myelin treatment compared to the vehicle (Fig. 4C). However, ELOVL1 inhibition did not alter the LD size (Fig. 4D). Noteworthy, due to the extensive foaminess of macrophages following sustained myelin exposure, quantification of the amount and size of the LDs is not reliable. Furthermore, the abundance of neutral lipids analyzed by BODIPY was unchanged after treatment with ELOVL1 inhibitor and myelin compared to the vehicle (Fig. 4E).

Given these findings on lipid metabolism, we further investigated the impact of ELOVL1 inhibition on myelin internalization by macrophages. Accordingly, BMDMs were treated with ELOVL1 inhibitor or vehicle for 24 h and 72 h, and subsequently exposed to fluorescently (DiI)-labeled myelin for 1.5 h to examine the uptake. ELOVL1 inhibition for 24 h augmented the percentage of phagocytosing BMDMs, while 72 h of treatment decreased it compared to the vehicle condition (Fig. 4F). Additionally, BMDMs that received 72 h ELOVL1 inhibitor treatment showed a significantly reduced MFI of DiI-myelin, indicating that the phagocytizing cells took up less myelin when compared to the vehicle (Fig. 4G). Furthermore, we evaluated the gene expression of low-density lipoprotein receptor-related protein (*Lrp)1* and scavenger receptor *Cd36* after ELOVL1 inhibition. LRP1 has been shown to be an important receptor for the uptake of myelin in phagocytes (42). In addition, our research group showed that FA translocase CD36 is essential for clearing myelin debris by phagocytes in MS (43). Specifically, ELOVL1 inhibition of 24 h markedly reduced the expression of *Cd36* and *Lrp1* in the absence of myelin (Fig. 4H).

Next, we investigated if ELOVL1 inhibition influences the efflux of lipids by macrophages.

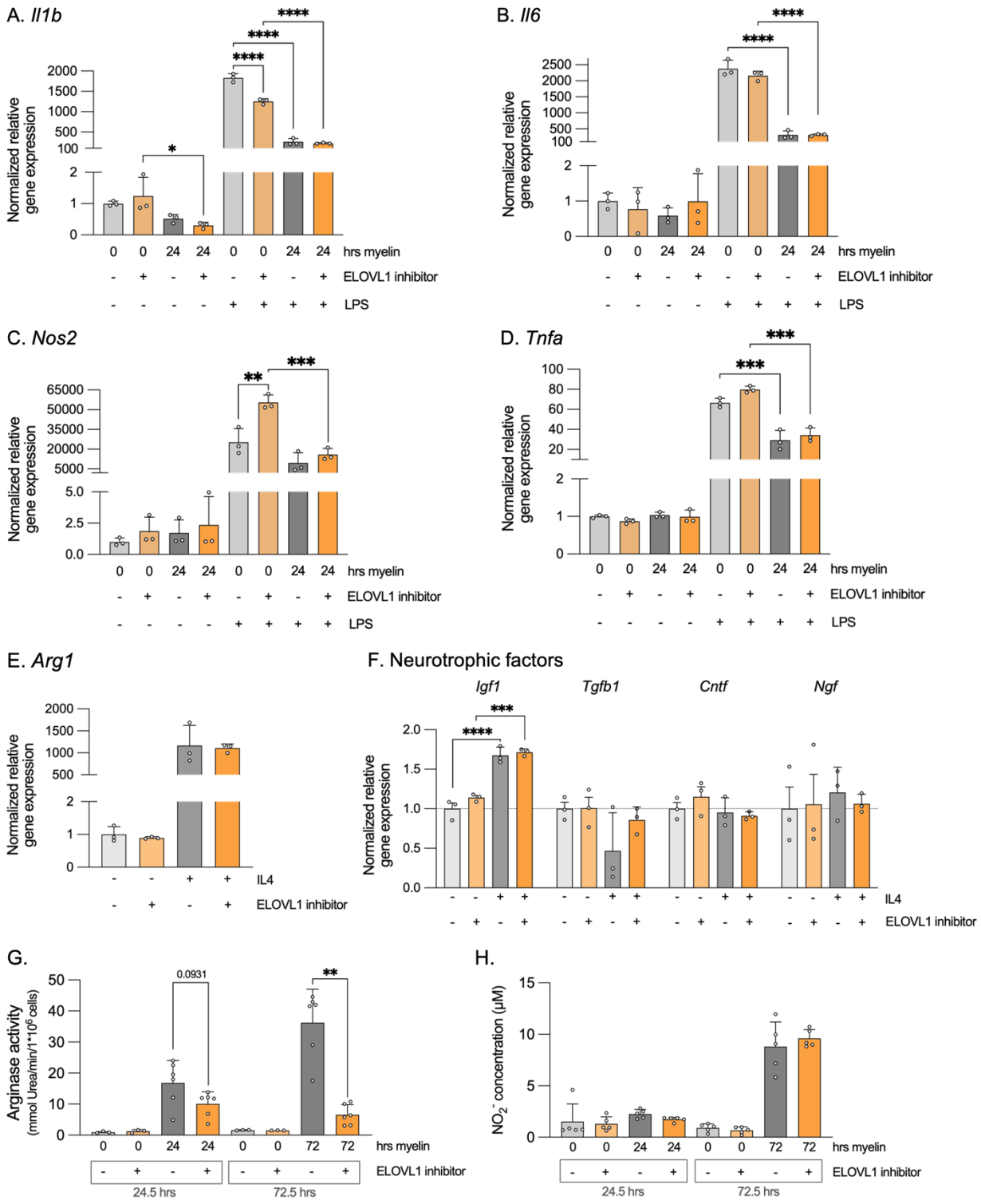

Fig. 3 – ELOVL1 inhibition influences the inflammatory phenotype of macrophages. (A-D) Gene expression of inflammatory genes including (A) interleukin (*Il)1b*, (B) *Il6*, (C) nitric oxide synthase 2 (*Nos2*), and (D) tumor necrosis factor α (*Tnfa*) in BMDMs pre-treated with 8 µM of ELOVL1 inhibitor (+) or vehicle (–) for 30 min, followed by a 24 h myelin exposure and subsequently with or without

Fig. 3 – Continued
a 6 h lipopolysaccharide (LPS) induction (n = 3 wells). **(E, F)** Gene expression of (E) arginase 1 (*Arg1*) and (F) neurotrophic factors (insulin growth factor 1 [*Igf1*], tumor growth factor β [*Tgfb1*], ciliary neurotrophic factor [*Cntf*], nerve growth factor [*Ngf*]) in BMDMs treated with 8 μM of ELOVL1 inhibitor (+) or vehicle (–) for 24 h, with or without a subsequent IL4 stimulation for 24 h (n = 3 wells). **(G)** Arginase activity in cell lysates from BMDMs treated with 8 μM of ELOVL1 inhibitor (+) or vehicle (–) and myelin for 24 h or 72 h, followed by 24 h stimulation with IL4 (n = 3-6 wells). **(H)** NO_2^- levels in supernatants from BMDMs treated with 8 μM of ELOVL1 inhibitor (+) or vehicle (–) and myelin for 24 h or 72 h, followed by LPS stimulation for 18 h (n = 5 wells). Data are represented as mean ± SD. *, P < 0.05; **, P < 0.01; ***, P < 0.001; ****, P < 0.0001; (A-F) one-way ANOVA, (G, H) Mann-Whitney.

The ATP Binding Cassette subfamily A member 1 (ABCA1) and subfamily G member 1 (ABCG1)-mediated cholesterol efflux has been shown to be important in controlling cholesterol load in phagocytes (44, 45). Therefore, we investigated the *Abca1* and *Abcg1* expression in macrophages treated with ELOVL1 inhibitor. In BMDMs without myelin stimulation, ELOVL1 inhibition significantly decreases *Abca1* gene expression (Fig. 5A). This effect was absent after 24 h of myelin exposure (Fig. 5A). ELOVL1 inhibition did not reduce the *Abcg1* expression without myelin stimulation (Fig. 5A). However, acute myelin exposure significantly increased its expression in ELOVL1 inhibitor treated BMDMs compared to the absence of myelin (Fig. 5A). In correspondence with our findings at gene level, flow cytometric analysis of surface ABCA1 showed a reduced abundance after both 24.5 h (P = 0.0690) and 72.5 h treatment with the ELOVL1 inhibitor (Fig. 5B). Additionally, inhibition of ELOVL1 resulted in a trend (P = 0.0987) toward an increased ABCA1 abundance following prolonged myelin exposure (Fig. 5B), suggesting an enhancement in lipid efflux after treatment with the ELOVL1 inhibitor in foamy macrophages. Subsequently, ABCA1 staining was conducted on permeabilized BMDMs to visualize intracellular ABCA1. Notably, the nucleus exhibited strong staining for ABCA1 (Fig. 5C), resulting in its exclusion during quantification. Contradictory, the MFI of ABCA1 was increased after the ELOVL1 inhibitor without myelin (Fig. 5D). These results suggest that the inhibition of ELOVL1 can induce alterations in lipid efflux, which are contingent upon the presence or absence of myelin stimulation. In conclusion, ELOVL1 seems to play a role in determining the metabolic phenotype of macrophages by altering the uptake and efflux of myelin.

ELOVL1 inhibition and LPS inflammatory stimulus influence the expression of Elovl1, Elovl2, Elovl5, Elovl6 and Elovl7 – As a next step, we aimed to elucidate the influence of inflammatory stimulation with LPS and the ELOVL1 inhibitor on the gene expression of all *Elovls* in BMDMs. To this end, BMDMs were either pre-treated with ELOVL1 inhibitor or vehicle and exposed to myelin for 24 h or left untreated. Subsequently, cells were incubated with or without LPS and gene expression of all *Elovls* was analyzed. As observed previously (20), the transcript levels of *Elovl3* and *Elovl4* were on the lower limit of detection and were, therefore, not included.

In macrophages that were not inflammatory activated, the expression of *Elovl1* and *Elovl7* was unchanged while Elovl6 expression was reduced upon myelin exposure compared to cells without myelin (Fig. 6A-C). Following LPS stimulation, *Elovl1* expression increased in the absence of myelin but decreased again after myelin exposure (Fig. 6A). *Elovl6* expression did not seem to change by LPS induction (Fig. 6B). In addition, LPS stimulation markedly reduced the expression of *Elovl7* (Fig. 6C). Myelin exposure slightly increased the *Elovl7* levels after ELOVL1 inhibitor in LPS-stimulated BMDMs compared to cells without myelin stimulation (Fig. 6C). When comparing the ELOVL1 inhibitor with the vehicle, ELOVL1 inhibition did not alter *Elovl1* levels, as expected (Fig. 6A). Interestingly, ELOVL1 inhibition significantly lowered *Elovl6* levels compared to the vehicle in LPS-stimulated BMDMs (Fig. 6B). Nevertheless, myelin stimulation diminishes its expression for both the

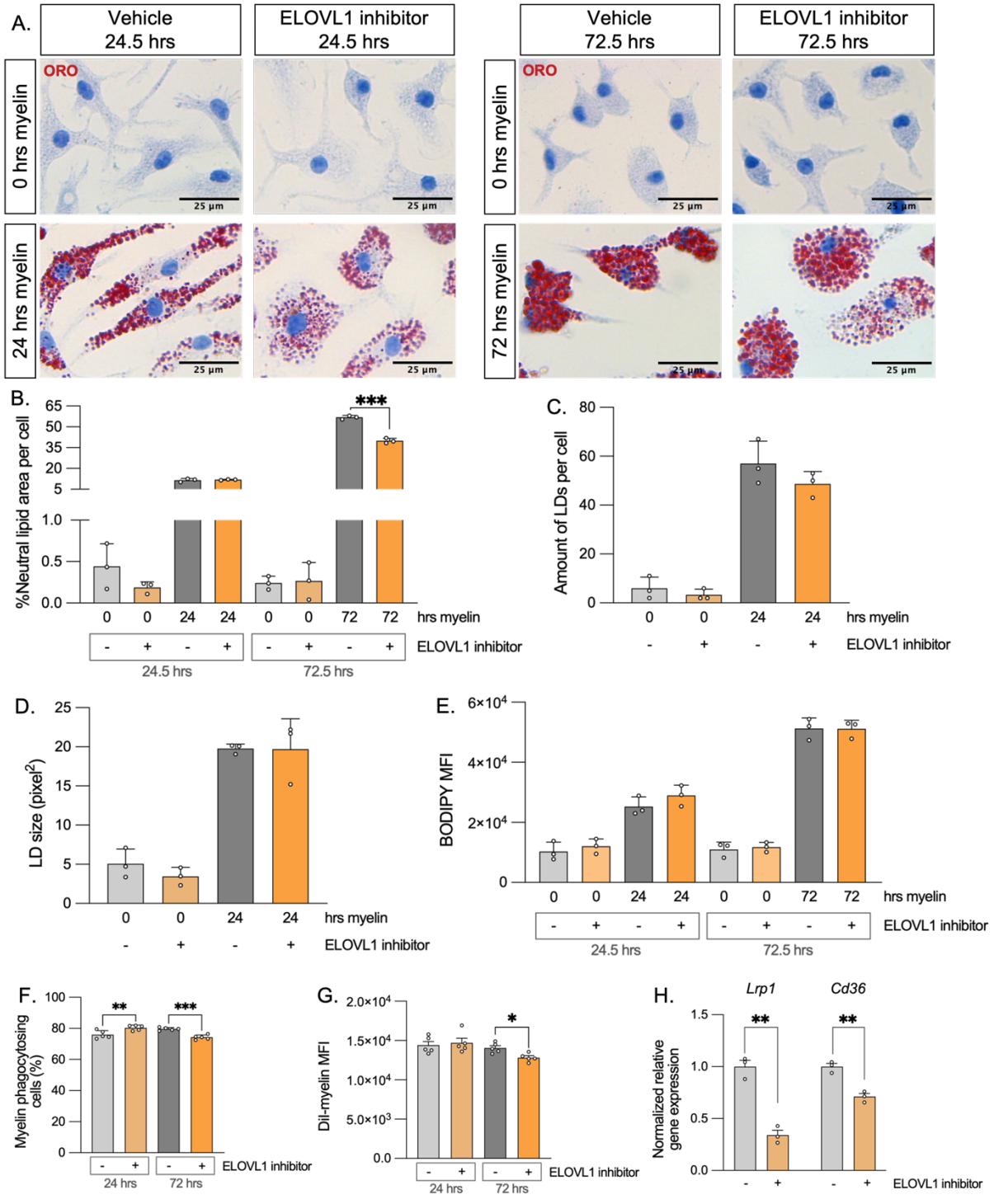

Fig. 4 – ELOVL1 inhibition impacts the metabolic phenotype of macrophages. (A) Oil red O (ORO) staining for neutral lipids of BMDMs treated with 8 µM of ELOVL1 inhibitor or vehicle (pre-treatment for 30 min) and myelin for 24 h or 72 h (Scale bar: 25 µm). **(B-D)** Quantification of (B) area of lipids per cell, (C) amount of lipid droplets (LDs) per cell, and (D) LD size based on ORO staining (n = 3 coverslips, 2-3 pictures per coverslip). The unit of pixel^2 corresponds to 0.071 µm^2. **(E)** Flow cytometry analysis of BODIPY median fluorescent intensity (MFI) in BMDMs treated with 4 µM of

Fig. 4 – Continued
ELOVL1 inhibitor (+) or vehicle (–) and myelin for 24 h or 72 h (n = 3 wells). **(F, G)** Phagocytosis assay on BMDMs treated with 8 µM of ELOVL1 inhibitor (+) or vehicle (–) for 24 h or 72 h, followed by exposure to DiI-labelled myelin for 1.5 h. Flow cytometric analysis of (F) the amount of myelin phagocytosing cells and (G) the mean fluorescent intensity (MFI) of DiI-myelin indicating the extent of myelin internalization in (n = 5 wells). **(H)** Gene expression of low-density lipoprotein receptor-related protein *(Lrp)1* and *Cd36* in BMDMs treated with 8 µM of ELOVL1 inhibitor or vehicle for 24 h (n = 3 wells). Data are represented as mean ± SD. *, P < 0.05; **, P < 0.01; ***, P < 0.001; (B, E) one-way ANOVA, (C, D, F-H) unpaired Student's t-test.

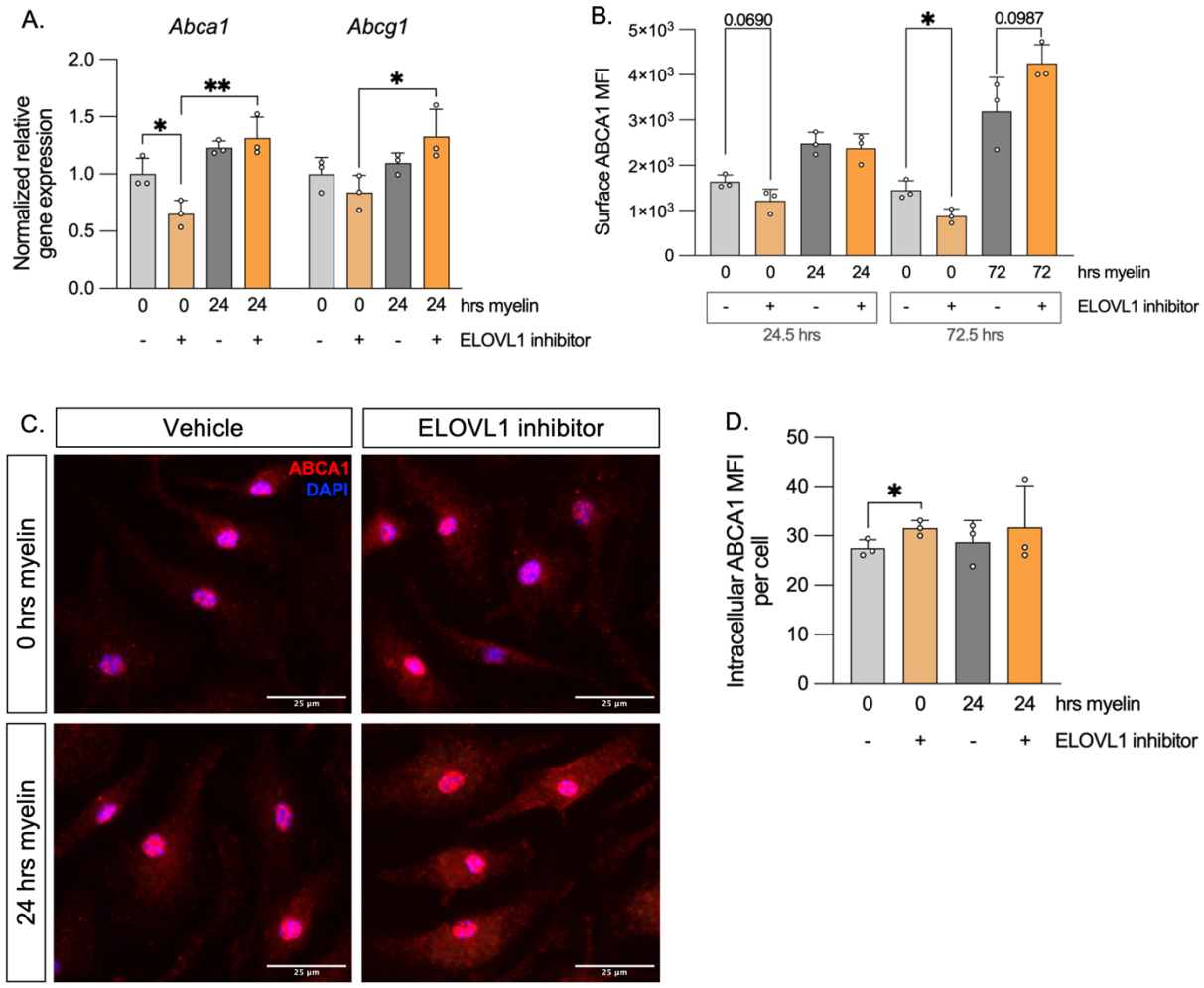

Fig. 5 – ELOVL1 inhibition alters ABCA1 expression in BMDMs. (A) Gene expression of *Abca1* and *Abcg1* in BMDMs pre-treated with 8 µM of ELOVL1 inhibitor (+) or vehicle (–) for 30 min, followed by a 24 h myelin exposure. **(B)** Flow cytometric analysis of surface ABCA1 abundance in BMDMs treated with 8 µM of ELOVL1 inhibitor (+) or vehicle (–) (30 min pre-treated) and myelin for 24 h or 72 h (n = 3 wells). **(C)** Representative images of intracellular ABCA1 staining of BMDMs treated with 8 µM of ELOVL1 inhibitor or vehicle (30 min pre-treated) and myelin for 24 h (Scale bar: 25 µm). **(D)** Quantification of intracellular ABCA1 mean fluorescent intensity (MFI) per cell based on ABCA1 fluorescent staining (n = 3 coverslips, 2 pictures per coverslip). Data are represented as mean ± SD. *, P < 0.05; **, P < 0.01; (A, B) one-way ANOVA, (D) unpaired Student's t-test.

ELOVL1 inhibitor and the vehicle, bringing it to a level similar to the vehicle condition without myelin (Fig. 6B). Furthermore, ELOVL1 inhibition did not impact the expression of Elovl7 (Fig. 6C).

On the other hand, the expression of *Elovls* involved in the elongation of PUFAs was also altered. LPS stimulation significantly enhanced *Elovl2* expression (Fig. 6D). Remarkably, LPS-stimulated cells treated with ELOVL1 inhibitor without myelin showed a markedly elevated *Elovl2* expression (Fig. 6D). In addition, no significant alterations in Elovl5 levels were detected, with only a downward trend ($P = 0.0569$) apparent after treatment with ELOVL1 inhibitor in LPS-stimulated cells (Fig. 6E). In conclusion, ELOVL1 inhibition seems to mainly affect the expression of *Elovls* after inflammatory stimulation in macrophages. Interestingly, not only the elongation of SFAs and MUFAs, in which ELOVL1 is involved, was impacted, but the expression of *Elovls* responsible for PUFA elongation was also altered.

Gene expression of Elovl5, but not Elovl1, is altered in OLs – In progressive MS, remyelination is limited as OPCs fail to differentiate into mature OLs (46). Hence, OPC differentiation and viability are essential for efficient remyelination. To elucidate if ELOVLs are altered OPCs and OLs, we investigated the expression of selected *Elovls* in OPCs (day 0 of differentiation), committed OLs (day 3), and mature OLs (day 6). The expression of myelin basic protein (*Mbp*) was significantly elevated in mature OLs (Fig. S3), indicating that OPC differentiation took successfully place. Gene expression analysis showed a slight trend toward lowered *Elovl1* levels in committed and mature OLs compared to OPCs (Fig. 7A). Notably, the expression of *Elovl5* diminished in both committed OPCs and mature OLs ($P = 0.0551$) compared to immature OPCs (Fig. 7A), indicating that ELOVL5 might play a role during OPC differentiation.

ELOVL1 inhibition stimulates ex vivo remyelination – Next, we aimed to elucidate the impact of ELOVL1 inhibition on remyelination in an *ex vivo* cerebellar BSC. This organotypic BSC model has demonstrated high fidelity in modeling the *in vivo* situation (47, 48). After lysolecithin-induced demyelination, brain slices were treated with ELOVL1 inhibitor or vehicle for 7 days, and remyelination was assessed by immunofluorescent staining for MBP and neurofilament (NF). Brain slices that received the ELOVL1 inhibitor showed a trend ($P = 0.0708$) toward a higher colocalization of MBP and axons (NF) compared to the vehicle (Fig. 7B, C). This indicates that ELOVL1 inhibition may potentially enhance remyelination upon lysolecithin-induced demyelination.

DISCUSSION

Both infiltrated macrophages and CNS-resident microglia play a pivotal role in MS pathology. These phagocytes can promote remyelination and CNS repair by producing neurotrophic factors and clearing myelin debris while also contributing to neurodegeneration and neuroinflammation by releasing inflammatory mediators (18). Understanding their dual roles is pivotal for developing effective MS therapies. In this study, we showed that inhibition of ELOVL1 alters the inflammatory and metabolic characteristics of macrophages. In addition, ELOVL1 suppression altered the expression of other *Elovls* in inflammatory-stimulated macrophages. Moreover, ELOVL1 inhibition appeared to promote remyelination in an *ex vivo* BSC model. Hereby, our findings present phagocyte-specific ELOVL1 inhibition as a potential strategy to promote remyelination in demyelinating disorders.

SFAs have been associated with increasing the inflammatory status of phagocytes (49, 50). Consequently, inhibiting ELOVL1 appears to be an interesting strategy to skew these phagocytes towards a less inflammatory phenotype. We observed that ELOVL1 inhibition lowered *Il1b* expression but enhanced *Nos2* expression in inflammatory-stimulated macrophages. However, 24 h of myelin stimulation reversed the higher *Nos2* levels, aligning with the described less inflammatory phenotype following acute myelin exposure (17). Further elucidation through studying the effects following sustained myelin exposure would provide valuable insights. In addition, emerging evidence suggests that phagocytes can promote remyelination by secreting neurotrophic mediators such as IGF1, TGF-β and CNTF, as they can stimulate OL survival and OPC differentiation (38, 51, 52). In this study, no alterations in the expression of these factors were detected in macrophages after ELOVL1 inhibition.

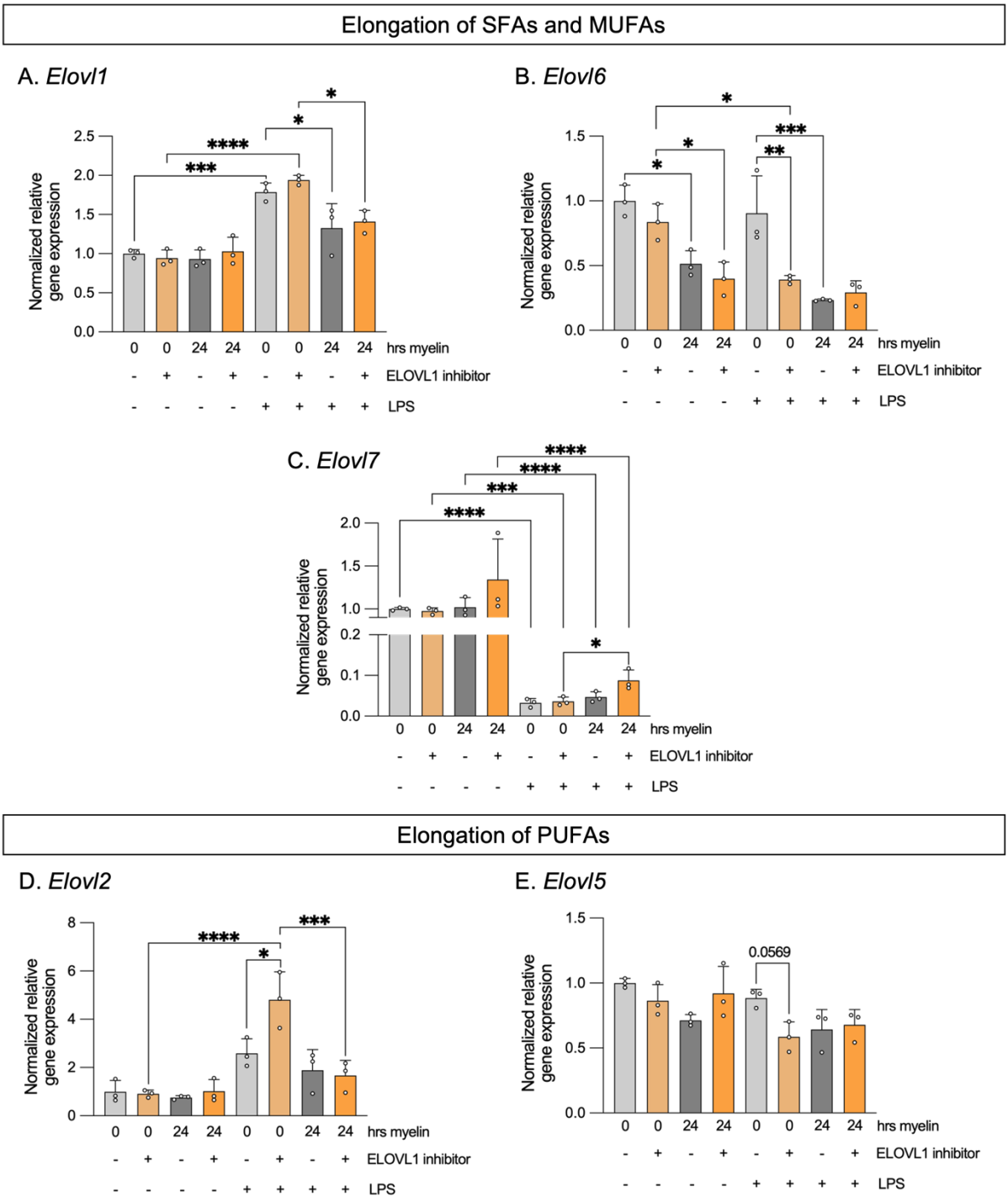

Fig. 6 – ELOVL1 inhibition and inflammatory stimulus influences the expression of *Elovl1*, *Elovl2*, *Elovl6* and *Elovl7*. BMDMs were pre-treated with 8 µM of ELOVL1 inhibitor (+) or vehicle (–) for 30 min, and subsequently treated with or without a 24 h myelin exposure and 6 h lipopolysaccharide (LPS) induction (n = 3 wells). **(A-C)** Gene expression of *Elovls* involved in the elongation of saturated (SFAs) and mono-unsaturated fatty acids (MUFAs), including (A) *Elovl1*, (B) *Elovl6*, and (C) *Elovl7*. **(D, E)** Gene expression of *Elovls* involved in the elongation of poly-unsaturated fatty acids (PUFAs), including (D) *Elovl2* and (E) *Elovl5*. Data are represented as mean ± SD. *, $P < 0.05$; **, $P < 0.01$; ***, $P < 0.001$; ****, $P < 0.0001$; one-way ANOVA.

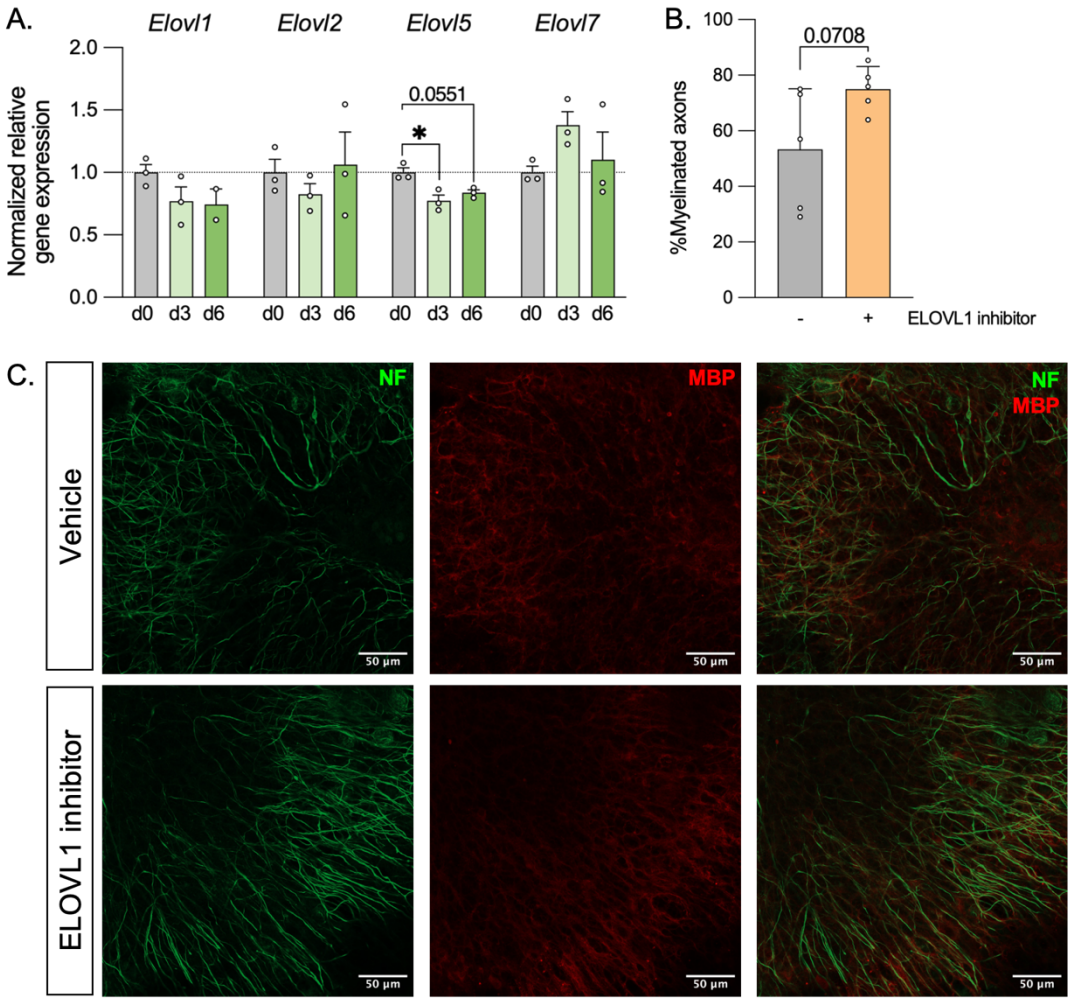

Fig. 7 – The expression of *Elovl5*, but not *Elovl1*, is altered in oligodendrocytes (OLs); ELOVL1 inhibition stimulates *ex vivo* remyelination. (A) Gene expression of *Elovl1*, *2*, *5*, and *7* in oligodendrocyte precursor cells (OPCs; day 0), committed oligodendrocytes (OLs; day 3) and mature OLs (day 6) (n = 3 wells). **(B)** Brain slice cultures (BSCs) were demyelinated, treated daily with 4 µM ELOVL1 inhibitor or vehicle for 7 days and stained for myelin basic protein (MBP) and neurofilament (NF). Percentage of $MBP^{+}NF^{+}$ axons out of total NF^{+} axons (n = 5 slices, 3 pictures per slice) was determined. **(C)** Representative immunofluorescence images of MBP/NF staining in BSCs (Scale bar: 50 µm). The images presented have been digitally enhanced under consistent settings. Data are represented as mean ± SD. *, $P < 0.05$; (A) one-way ANOVA and (B) unpaired Student's t-test.

Nonetheless, we observed that ELOVL1 inhibition led to a reduction in arginase activity in myelin-loaded macrophages, while levels of NO remained unaltered. These results indicate that ELOVL1 suppression has a modest effect on the inflammatory macrophage phenotype, favoring more pro-inflammatory features over less inflammatory ones. Nevertheless, further research on the impact of ELOVL1 on the inflammatory phagocyte features is necessary to draw definitive conclusions.

Given that sustained myelin internalization induces a shift in phagocytes towards an inflammatory phenotype, thereby impeding CNS repair (19), and recognizing that altered FA metabolism underlies this phenotypic shift (19, 20), we further elucidate the association between the elongation of SFAs by ELOVL1 and the metabolic

characteristics of macrophages. After prolonged myelin exposure, the administration of the ELOVL1 inhibitor resulted in reduced lipid load and myelin phagocytosis within macrophages. Additionally, we noted a decline in the expression of *Lrp1* and *Cd36*, crucial for myelin uptake, after ELOVL1 inhibition in macrophages lacking myelin. It would be of interest to delve deeper into the role of ELOVL1 in altering LRP1 and CD36, especially in myelin-loaded phagocytes. Furthermore, we show that macrophages treated with the ELOVL1 inhibitor had both a lower *Abca1* gene expression and ABCA1 abundance, suggesting that ELOVL1 inhibition hinders lipid efflux in the absence of myelin. It has been shown that ABCA1 deficiency can induce a pro-angiogenic phenotype in nonlipid-loaded macrophages by lowering the expression of inflammatory mediators (53). This suggests that ELOVL1 inhibition might potentially induce a less inflammatory phenotype through the modulation of ABCA1 levels. In addition, following ELOVL1 inhibitor treatment, ABCA1 abundance was enhanced after sustained myelin exposure. These results suggest that it stimulates the efflux of lipids in foamy macrophages. This increased ABCA1 abundance in macrophages was also observed after Elovl6 depletion (20). Recent findings have demonstrated that a diminished capacity to eliminate cholesterol derived from internalized myelin via ABCA1 triggers an inflammatory phagocyte phenotype that hampers CNS repair (19). Therefore, ELOVL1 suppression seems to be beneficial by improving lipid efflux and reducing lipid load in macrophages.

FA elongation plays a crucial role in shaping the cellular lipidome, influencing both homeostasis and disease states (54). We demonstrated that the expression of other *Elovls* is influenced by inflammatory stimulation and ELOVL1 inhibition. Some studies have identified links between immune responses and the activities of the ELOVL family, suggesting that ELOVLs play an important role in regulating the macrophage function. For instance, *Elovl6* deficiency reduced the expression of inflammatory genes while it increased the expression of various neurotrophic factors in macrophages stimulated with LPS, representing a less inflammatory macrophage phenotype (20). Specifically, we found that ELOVL1 inhibition downregulated the *Elovl6* expression in LPS-stimulated macrophages, implying a potential shift towards a less inflammatory phenotype as a consequence of the ELOVL1 inhibition. On the other hand, knockout of ELOVL2 induced a more inflammatory phenotype in M1 macrophages that were activated with LPS and IFNγ while M2 macrophages exhibited diminished protective effects (55). Therefore, the observed increase in Elovl2 expression following ELOVL1 inhibition in inflammatory-stimulated macrophages also suggests a potential modulation towards a less inflammatory phenotype mediated by the inhibition. Furthermore, ELOVL7 has been shown to be upregulated in M1 macrophages and is associated with the enhanced production of inflammatory cytokines (56). Here, no alterations in *Elovl7* expression were observed after ELOVL1 inhibition. This observation suggests that ELOVL7 may not compensate for the ELOVL1 suppression. In contrast, it is noteworthy that the stimulation with LPS led to an overall downregulation of *Elovl7* expression. Additional studies focusing on the impact of ELOVL1 inhibition and inflammatory activation in macrophages are necessary to clarify observed effects.

Clearance of myelin debris by phagocytes plays a pivotal role in facilitating the remyelination process, as it fosters OPC maturation and induces a shift in phagocytes towards a reparative phenotype. Here, we observed that inhibiting ELOVL1 seemed to ameliorate lysolecithin-induced demyelination in *ex vivo* brain slice culture. In contrast, Elovl1 knockout mice exhibited mild myelin thinning in the corpus callosum (57). In addition, patients with an ELOVL1 mutation present with hypomyelination (28, 58). However, ELOVL1 suppression in phagocytes specifically may indeed be beneficial for promoting remyelination. Nevertheless, it remains uncertain whether the observed effect is attributed to alterations in phagocytes, as the improvement may potentially involve other cell types. For instance, ELOVL1 has been positively associated with the inflammatory status of astrocytes in X-ALD (59). In addition, OLs of X-ALD patients exhibit pronounced expression of ELOVL1 and this elongase has been pinpointed to be accountable for catalyzing the detrimental buildup of VLCFAs (60, 61). Nevertheless, further research should be conducted to unravel the role of ELOVL1 in other CNS cell types.

Future research directions could focus on elucidating the specific alterations in lipid metabolism induced by ELOVL1 inhibition. To address this, innovative lipidomic analyses could be employed to identify changes in FA species following treatment with the ELOVL1 inhibitor in macrophages. Additionally, investigations into potential shifts in the pathway toward increased elongation of PUFAs or MUFAs could provide further insights. Furthermore, considering the evidence suggesting that *Elovl6* deficiency altered the balance in the desaturation index of various lipid species (20), it is relevant to assess potential differences in desaturation through ELOVL1 inhibition. Another aspect of future research could involve unraveling the underlying pathways altered by ELOVL1 inhibition. Our research group has previously demonstrated that *Elovl6* depletion in macrophages enhances peroxisome proliferator-activated receptor (PPAR)γ activity, and that the decrease in ABCA1 abundance is regulated by PPARγ (20). Activation of PPARγ has been shown to reduce the activation of innate immune cells and inhibit foam cell formation while promoting macrophage polarization towards an anti-inflammatory phenotype (37, 62-64). Given our observation of reduced ABCA1 abundance following ELOVL1 inhibition, it is plausible that ELOVL1 inhibition may also trigger the activation of PPARγ. In addition, activation of PPARα has been shown to modulate the expression of ELOVL1 and ELOVL6 (26). Considering that PPARα activation shares similar anti-inflammatory effects on macrophages as PPARγ and can elevate ABCA1 expression (64-66), exploration of its role in modulating ELOVL1 in the context of MS presents another intriguing avenue for investigation. In summary, unraveling these potential lipidome and pathway alterations could provide valuable insights into the molecular mechanism resulting from ELOVL1 inhibition and its impact on macrophage function, inflammation and remyelination.

CONCLUSION

In conclusion, this study provides initial insights into the involvement of ELOVL1 in shaping the inflammatory and metabolic phenotype of macrophages in the context of MS. Further studies are necessary to deepen our understanding. Nevertheless, the findings of this study suggest that modulating FA metabolism through ELOVL inhibition in phagocytes can present a promising strategy to enhance remyelination in demyelinating diseases such as MS.

REFERENCES

1. Walton C, King R, Rechtman L, Kaye W, Leray E, Marrie RA, et al. Rising prevalence of multiple sclerosis worldwide: Insights from the Atlas of MS, third edition. Mult Scler. 2020;26(14):1816-21.
2. Filippi M, Bar-Or A, Piehl F, Preziosa P, Solari A, Vukusic S, et al. Multiple sclerosis. Nat Rev Dis Primers. 2018;4(1):43.
3. Dobson R, Giovannoni G. Multiple sclerosis - a review. Eur J Neurol. 2019;26(1):27-40.
4. Dendrou CA, Fugger L, Friese MA. Immunopathology of multiple sclerosis. Nat Rev Immunol. 2015;15(9):545-58.
5. Olsen JA, Akirav EM. Remyelination in multiple sclerosis: cellular mechanisms and novel therapeutic approaches. J Neurosci Res. 2015;93(5):687-96.
6. Popescu BF, Lucchinetti CF. Meningeal and cortical grey matter pathology in multiple sclerosis. BMC Neurol. 2012;12:11.
7. Ghasemi N, Razavi S, Nikzad E. Multiple Sclerosis: Pathogenesis, Symptoms, Diagnoses and Cell-Based Therapy. Cell J. 2017;19(1):1-10.
8. Bruck W, Kuhlmann T, Stadelmann C. Remyelination in multiple sclerosis. J Neurol Sci. 2003;206(2):181-5.
9. Hagemeier K, Bruck W, Kuhlmann T. Multiple sclerosis - remyelination failure as a cause of disease progression. Histol Histopathol. 2012;27(3):277-87.
10. Staugaitis SM, Chang A, Trapp BD. Cortical pathology in multiple sclerosis: experimental approaches to studies on the mechanisms of demyelination and remyelination. Acta Neurol Scand Suppl. 2012(195):97-102.
11. Kipp M, Victor M, Martino G, Franklin RJ. Endogeneous remyelination: findings in human studies. CNS Neurol Disord Drug Targets. 2012;11(5):598-609.
12. Frahm N, Hecker M, Zettl UK. Polypharmacy in patients with multiple sclerosis: a gender-specific analysis. Biol Sex Differ. 2019;10(1):27.
13. Absinta M, Sati P, Masuzzo F, Nair G, Sethi V, Kolb H, et al. Association of Chronic Active Multiple Sclerosis Lesions With Disability In Vivo. JAMA Neurol. 2019;76(12):1474-83.

14. Kaunzner UW, Kang Y, Zhang S, Morris E, Yao Y, Pandya S, et al. Quantitative susceptibility mapping identifies inflammation in a subset of chronic multiple sclerosis lesions. Brain. 2019;142(1):133-45.
15. Bogie JF, Timmermans S, Huynh-Thu VA, Irrthum A, Smeets HJ, Gustafsson JA, et al. Myelin-derived lipids modulate macrophage activity by liver X receptor activation. PLoS One. 2012;7(9):e44998.
16. Lloyd AF, Miron VE. The pro-remyelination properties of microglia in the central nervous system. Nat Rev Neurol. 2019;15(8):447-58.
17. Boven LA, Van Meurs M, Van Zwam M, Wierenga-Wolf A, Hintzen RQ, Boot RG, et al. Myelin-laden macrophages are anti-inflammatory, consistent with foam cells in multiple sclerosis. Brain. 2006;129(Pt 2):517-26.
18. Bogie JF, Stinissen P, Hendriks JJ. Macrophage subsets and microglia in multiple sclerosis. Acta Neuropathol. 2014;128(2):191-213.
19. Bogie JFJ, Grajchen E, Wouters E, Corrales AG, Dierckx T, Vanherle S, et al. Stearoyl-CoA desaturase-1 impairs the reparative properties of macrophages and microglia in the brain. J Exp Med. 2020;217(5).
20. Garcia Corrales AV, Verberk SGS, Haidar M, Grajchen E, Dehairs J, Vanherle S, et al. Fatty acid elongation by ELOVL6 hampers remyelination by promoting inflammatory foam cell formation during demyelination. Proc Natl Acad Sci U S A. 2023;120(37):e2301030120.
21. Guillou H, Zadravec D, Martin PG, Jacobsson A. The key roles of elongases and desaturases in mammalian fatty acid metabolism: Insights from transgenic mice. Prog Lipid Res. 2010;49(2):186-99.
22. Nakamura MT, Yudell BE, Loor JJ. Regulation of energy metabolism by long-chain fatty acids. Prog Lipid Res. 2014;53:124-44.
23. Ecker J, Liebisch G, Englmaier M, Grandl M, Robenek H, Schmitz G. Induction of fatty acid synthesis is a key requirement for phagocytic differentiation of human monocytes. Proc Natl Acad Sci U S A. 2010;107(17):7817-22.
24. Karasawa T, Kawashima A, Usui-Kawanishi F, Watanabe S, Kimura H, Kamata R, et al. Saturated Fatty Acids Undergo Intracellular Crystallization and Activate the NLRP3 Inflammasome in Macrophages. Arterioscler Thromb Vasc Biol. 2018;38(4):744-56.
25. Wallner S, Grandl M, Konovalova T, Sigruner A, Kopf T, Peer M, et al. Monocyte to macrophage differentiation goes along with modulation of the plasmalogen pattern through transcriptional regulation. PLoS One. 2014;9(4):e94102.
26. Wang X, Yu H, Gao R, Liu M, Xie W. A comprehensive review of the family of very-long-chain fatty acid elongases: structure, function, and implications in physiology and pathology. Eur J Med Res. 2023;28(1):532.
27. Chrast R, Saher G, Nave KA, Verheijen MH. Lipid metabolism in myelinating glial cells: lessons from human inherited disorders and mouse models. J Lipid Res. 2011;52(3):419-34.
28. Kutkowska-Kazmierczak A, Rydzanicz M, Chlebowski A, Klosowska-Kosicka K, Mika A, Gruchota J, et al. Dominant ELOVL1 mutation causes neurological disorder with ichthyotic keratoderma, spasticity, hypomyelination and dysmorphic features. J Med Genet. 2018;55(6):408-14.
29. Zierfuss B, Buda A, Villoria-Gonzalez A, Logist M, Fabjan J, Parzer P, et al. Saturated very long-chain fatty acids regulate macrophage plasticity and invasiveness. J Neuroinflammation. 2022;19(1):305.
30. Bogie JF, Mailleux J, Wouters E, Jorissen W, Grajchen E, Vanmol J, et al. Scavenger receptor collectin placenta 1 is a novel receptor involved in the uptake of myelin by phagocytes. Sci Rep. 2017;7:44794.
31. Weischenfeldt J, Porse B. Bone Marrow-Derived Macrophages (BMM): Isolation and Applications. CSH Protoc. 2008;2008:pdb prot5080.
32. Loix M, Wouters E, Vanherle S, Dehairs J, McManaman JL, Kemps H, et al. Perilipin-2 limits remyelination by preventing lipid droplet degradation. Cell Mol Life Sci. 2022;79(10):515.
33. Vanherle S, Guns J, Loix M, Mingneau F, Dierckx T, Wouters F, et al. Extracellular vesicle-associated cholesterol supports the regenerative functions of macrophages in the brain. J Extracell Vesicles. 2023;12(12):e12394.
34. Norton WT, Poduslo SE. Myelination in rat brain: changes in myelin composition during brain maturation. J Neurochem. 1973;21(4):759-73.
35. Hussain R, El-Etr M, Gaci O, Rakotomamonjy J, Macklin WB, Kumar N, et al. Progesterone and Nestorone facilitate axon remyelination: a role for

progesterone receptors. Endocrinology. 2011;152(10):3820-31.
36. Meffre D, Massaad C, Grenier J. Lithium chloride stimulates PLP and MBP expression in oligodendrocytes via Wnt/beta-catenin and Akt/CREB pathways. Neuroscience. 2015;284:962-71.
37. Bogie JF, Jorissen W, Mailleux J, Nijland PG, Zelcer N, Vanmierlo T, et al. Myelin alters the inflammatory phenotype of macrophages by activating PPARs. Acta Neuropathol Commun. 2013;1:43.
38. Rawji KS, Mishra MK, Yong VW. Regenerative Capacity of Macrophages for Remyelination. Front Cell Dev Biol. 2016;4:47.
39. Boyd MJ, Collier PN, Clark MP, Deng H, Kesavan S, Ronkin SM, et al. Discovery of Novel, Orally Bioavailable Pyrimidine Ether-Based Inhibitors of ELOVL1. J Med Chem. 2021;64(24):17777-94.
40. Verberk SGS, de Goede KE, Gorki FS, van Dierendonck X, Arguello RJ, Van den Bossche J. An integrated toolbox to profile macrophage immunometabolism. Cell Rep Methods. 2022;2(4):100192.
41. Rosas-Ballina M, Guan XL, Schmidt A, Bumann D. Classical Activation of Macrophages Leads to Lipid Droplet Formation Without de novo Fatty Acid Synthesis. Front Immunol. 2020;11:131.
42. Grajchen E, Hendriks JJA, Bogie JFJ. The physiology of foamy phagocytes in multiple sclerosis. Acta Neuropathol Commun. 2018;6(1):124.
43. Grajchen E, Wouters E, van de Haterd B, Haidar M, Hardonniere K, Dierckx T, et al. CD36-mediated uptake of myelin debris by macrophages and microglia reduces neuroinflammation. J Neuroinflammation. 2020;17(1):224.
44. Kennedy MA, Barrera GC, Nakamura K, Baldan A, Tarr P, Fishbein MC, et al. ABCG1 has a critical role in mediating cholesterol efflux to HDL and preventing cellular lipid accumulation. Cell Metab. 2005;1(2):121-31.
45. Vanherle S, Jorissen W, Dierckx T, Loix M, Grajchen E, Mingneau F, et al. The ApoA-I mimetic peptide 5A enhances remyelination by promoting clearance and degradation of myelin debris. Cell Rep. 2022;41(6):111591.
46. Fancy SP, Kotter MR, Harrington EP, Huang JK, Zhao C, Rowitch DH, et al. Overcoming remyelination failure in multiple sclerosis and other myelin disorders. Exp Neurol. 2010;225(1):18-23.
47. Miron VE, Ludwin SK, Darlington PJ, Jarjour AA, Soliven B, Kennedy TE, et al. Fingolimod (FTY720) enhances remyelination following demyelination of organotypic cerebellar slices. Am J Pathol. 2010;176(6):2682-94.
48. Zhang H, Jarjour AA, Boyd A, Williams A. Central nervous system remyelination in culture--a tool for multiple sclerosis research. Exp Neurol. 2011;230(1):138-48.
49. Anderson EK, Hill AA, Hasty AH. Stearic acid accumulation in macrophages induces toll-like receptor 4/2-independent inflammation leading to endoplasmic reticulum stress-mediated apoptosis. Arterioscler Thromb Vasc Biol. 2012;32(7):1687-95.
50. Camell C, Smith CW. Dietary oleic acid increases m2 macrophages in the mesenteric adipose tissue. PLoS One. 2013;8(9):e75147.
51. Kotter MR, Zhao C, van Rooijen N, Franklin RJ. Macrophage-depletion induced impairment of experimental CNS remyelination is associated with a reduced oligodendrocyte progenitor cell response and altered growth factor expression. Neurobiol Dis. 2005;18(1):166-75.
52. Miron VE, Boyd A, Zhao JW, Yuen TJ, Ruckh JM, Shadrach JL, et al. M2 microglia and macrophages drive oligodendrocyte differentiation during CNS remyelination. Nat Neurosci. 2013;16(9):1211-8.
53. Sene A, Khan AA, Cox D, Nakamura RE, Santeford A, Kim BM, et al. Impaired cholesterol efflux in senescent macrophages promotes age-related macular degeneration. Cell Metab. 2013;17(4):549-61.
54. Bogie JFJ, Haidar M, Kooij G, Hendriks JJA. Fatty acid metabolism in the progression and resolution of CNS disorders. Adv Drug Deliv Rev. 2020;159:198-213.
55. Talamonti E, Pauter AM, Asadi A, Fischer AW, Chiurchiu V, Jacobsson A. Impairment of systemic DHA synthesis affects macrophage plasticity and polarization: implications for DHA supplementation during inflammation. Cell Mol Life Sci. 2017;74(15):2815-26.
56. Inoue Y, Kamiya T, Hara H. Increased expression of ELOVL7 contributes to production of inflammatory cytokines in THP-1 cell-derived M1-like macrophages. J Clin Biochem Nutr. 2023;72(3):215-24.

57. Isokawa M, Sassa T, Hattori S, Miyakawa T, Kihara A. Reduced chain length in myelin sphingolipids and poorer motor coordination in mice deficient in the fatty acid elongase Elovl1. FASEB Bioadv. 2019;1(12):747-59.
58. Mueller N, Sassa T, Morales-Gonzalez S, Schneider J, Salchow DJ, Seelow D, et al. De novo mutation in ELOVL1 causes ichthyosis, acanthosis nigricans, hypomyelination, spastic paraplegia, high frequency deafness and optic atrophy. J Med Genet. 2019;56(3):164-75.
59. Guttenplan KA, Weigel MK, Prakash P, Wijewardhane PR, Hasel P, Rufen-Blanchette U, et al. Neurotoxic reactive astrocytes induce cell death via saturated lipids. Nature. 2021;599(7883):102-7.
60. Ofman R, Dijkstra IM, van Roermund CW, Burger N, Turkenburg M, van Cruchten A, et al. The role of ELOVL1 in very long-chain fatty acid homeostasis and X-linked adrenoleukodystrophy. EMBO Mol Med. 2010;2(3):90-7.
61. Singh J, Khan M, Pujol A, Baarine M, Singh I. Histone deacetylase inhibitor upregulates peroxisomal fatty acid oxidation and inhibits apoptotic cell death in abcd1-deficient glial cells. PLoS One. 2013;8(7):e70712.
62. Storer PD, Xu J, Chavis J, Drew PD. Peroxisome proliferator-activated receptor-gamma agonists inhibit the activation of microglia and astrocytes: implications for multiple sclerosis. J Neuroimmunol. 2005;161(1-2):113-22.
63. Ricote M, Valledor AF, Glass CK. Decoding transcriptional programs regulated by PPARs and LXRs in the macrophage: effects on lipid homeostasis, inflammation, and atherosclerosis. Arterioscler Thromb Vasc Biol. 2004;24(2):230-9.
64. Rigamonti E, Chinetti-Gbaguidi G, Staels B. Regulation of macrophage functions by PPAR-alpha, PPAR-gamma, and LXRs in mice and men. Arterioscler Thromb Vasc Biol. 2008;28(6):1050-9.
65. Bougarne N, Weyers B, Desmet SJ, Deckers J, Ray DW, Staels B, et al. Molecular Actions of PPARalpha in Lipid Metabolism and Inflammation. Endocr Rev. 2018;39(5):760-802.
66. Grabacka M, Pierzchalska M, Plonka PM, Pierzchalski P. The Role of PPAR Alpha in the Modulation of Innate Immunity. Int J Mol Sci. 2021;22(19).

Acknowledgements **–** I would like to extend my heartfelt gratitude to my daily supervisor, Tine Weytjens, for her unwavering guidance and support throughout my internship. Her insights and encouragement have been invaluable. I also express my sincere thanks to Dr. Sanne Verberk and Prof. Dr. Jerome Hendriks for their mentorship, support, and constructive feedback during this period. Their expertise contributed significantly to enhancing my critical thinking and research skills. I am also grateful to the other members of the research team for their assistance with lab work and the insightful feedback provided during our weekly lab meetings. I would like to acknowledge the Advanced Optical Microscopy Centre at Hasselt University for support with the microscopy experiments. Microscopy was made possible by the Research Foundation Flanders (Large Research Infrastructure Grant I001222N). A special thank you to Sam Vanherle, who provided me with RNA samples of OPCs. I would like to express my gratitude to my fellow students for fostering a supportive and stimulating environment. Our discussions significantly enriched my learning experience. Lastly, I am deeply grateful for the unwavering support from my friends and family throughout this internship and the past five years of my studies at UHasselt.

Author contributions – TW, SV, and JH designed the research. ES performed experiments and data analysis under the supervision of TW. TW and SV assisted with FACS. ES wrote the manuscript. TW, SV, and JH revised the manuscript.

This text is supported by GenAI.

SUPPLEMENTARY MATERIALS AND METHODS

Cerebellar brain slices isolation – Cerebellar brains were obtained from wild-type C57BL/6J mouse pups at postnatal day 10 and 200- 300 µm sagittal slices were made, as described previously (35, 36). Brain slices were cultured in MEM medium supplemented with 25% horse serum, 25% Hank's balanced salt solution, 50 U/mL penicillin/streptomycin, 1% glutamax, 12.5 mM HEPES and 1.45 g/L glucose.

Primary mouse OPCs – Primary mouse OPCs were isolated from postnatal day 0 to 2 C57BL/6J pups using the orbital shake-off method. Briefly, cerebral cortices were enzymatically dissociated for 20 min at 37°C with papain (3 U/mL; diluted in DMEM and supplemented with 1 mM L-cysteine) and 20 µg/mL DNase I. Subsequently, the isolated mixed glial cells were cultured in DMEM supplemented with 10% FCS, 50 U/mL penicillin/streptomycin in Poly-L-lysine (PLL, 50 µg/mL)-coated T75 culture flasks in an atmosphere of 37°C and 8.5% CO_2. On days 4, 7, and 11, medium was changed, and starting from day 7, bovine insulin (5 µg/mL) was added to the cultures. On day 14, the shake-off was performed: cultures were first shaken at 75 rpm and 37°C for 45 min to detach microglia, followed by shaking at 250 rpm and 37°C for 16 h to detach OPCs. The OPC-containing supernatant was then incubated on a petri dish for 20 min at 37°C and centrifuged at 300 g. Next, OPCs were seeded in PLL-coated wells at a density of 3 x 10^5 cells/ml, maintained in SATO proliferation medium (DMEM supplemented with 50 U/mL penicillin/streptomycin, 2% horse serum, 0.1 mM putrescine, 0.3 mM transferrin, 0.2 µM sodium selenite, 0.5 mM L-thyroxin, 0.02 mM progesterone, 0.8 mM bovine insulin, 0.5 µM triiodothyronine, 2% B27 supplement, 5 ng/µL platelet-derived growth factor α (PDGFα) and 5 ng/µL fibroblast growth factor (FGF)) for 2 days. Next, OPCs were cultured in differentiation medium (SATO medium lacking PDGFα and FGF) for 6 days.

Table S1 – List of reagents

Reagents	Supplier
α-isonitrosopropiophenone	Sigma-Aldrich, Bornem, Belgium
B27 supplement	In house production as described by Chen et al.
Bovine insulin	Sigma-Aldrich, Bornem, Belgium
DAPI	Invitrogen, Merelbeke, Belgium
DiI	Sigma-Aldrich, Bornem, Belgium
DMEM high glucose medium	Sigma-Aldrich, Bornem, Belgium
Dried skimmed milk powder	Marvel, Dublin, Ireland
EDTA	Lonza, Vervier, Belgium
ELOVL1-22	GLPBio, Montclair, USA (cat. GC49897)
Enhanced chemiluminescence Plus detection kit	Thermo Fisher Scientific, Erembodegem, Belgium
FCS	Biowest, Nuaillé, France
FGF	Peprotech, Hamburg, Germany
Glucose	Sigma-Aldrich, Bornem, Belgium
Glutamax	Thermo Fisher Scientific, Erembodegem, Belgium
H_2SO_4	Merck, Darmstadt, Germany
H_3PO_4	Merck, Darmstadt, Germany
Hank's balanced salt solution	Sigma-Aldrich, Bornem, Belgium
Hematoxylin	Mayer via Sigma-Aldrich, Bornem, Belgium
HEPES	Thermo Fisher Scientific, Erembodegem, Belgium
Horse serum	Sigma-Aldrich, Bornem, Belgium
IL4	Peprotech, Hamburg, Germany
L-arginine	Fluka, Buchs, Switzerland
L-thyroxin	Sigma-Aldrich, Bornem, Belgium
LPS	Sigma-Aldrich, Bornem, Belgium
Lysolecithin	Sigma-Aldrich, Bornem, Belgium
MEM medium	Thermo Fisher Scientific, Erembodegem, Belgium
$MnCl_2$	Sigma-Aldrich, Bornem, Belgium
N-(1-Naphthyl)ethylenediamine dihydrochloride	Sigma-Aldrich, Bornem, Belgium
ORO	Sigma-Aldrich, Bornem, Belgium
Papain	Sigma-Aldrich, Bornem, Belgium
PDGFα	Peprotech, Hamburg, Germany
Penicillin/streptomycin	Sigma-Aldrich, Bornem, Belgium
Pierce BCA protein assay kit	Thermo Fisher Scientific, Erembodegem, Belgium
Progesterone	Sigma-Aldrich, Bornem, Belgium
Protease inhibitor cocktail	Roche, Mannheim, Germany
Putrescine	Sigma-Aldrich, Bornem, Belgium
QIAzol	Qiagen, Venlo, The Netherlands
qScript™ cDNA SuperMix	Quanta Biosciences, Gaithersburg, USA
QuickStain Protein labeling kit	Amersham, Buckinghamshire, UK
RNeasy mini kit	Qiagen, Venlo, The Netherlands
RPMI 1640 medium	Gibco, Merelbeke, Belgium

Sodium selenite	Sigma-Aldrich, Bornem, Belgium
Sulfanilamide	Sigma-Aldrich, Bornem, Belgium
SYBR green master mix	Applied Biosystems, Gaasbeek, Belgium
Transferrin	Sigma-Aldrich, Bornem, Belgium
Triiodothyronine	Sigma-Aldrich, Bornem, Belgium
Tris-HCl	Sigma-Aldrich, Bornem, Belgium
Triton X-100	Sigma-Aldrich, Bornem, Belgium
Tween-20	Thermo Fisher Scientific, Erembodegem, Belgium

DAPI: 4,6′-diamidino-2-phenylindole, DiI: 3,3,39,39-tetramethylindocarbocyanine perchlorate, ELOVL: Elongation of very long-chain fatty acids proteins, FCS: Fetal calf serum, FGF: fibroblast growth factor, IL: Interleukin, LPS: lipopolysaccharide, ORO: Oil Red O, PDGFα: Platelet-derived growth factor α.

Table S2 – List of primer sequences for quantitative PCR

	Forward primer (5' → 3')	Reverse primer (5' → 3')
Abca1	CCCAGAGCAAAAAGCGACTC	GGTCATCATCACTTTGGTCCTTG
Abcg1	CAAGACCCTTTTGAAAGGGATCTC	GCCAGAATATTCATGAGTGTGGAC
Arg1	GTGAAGAACCCACGGTCTGT	GCCAGAGATGCTTCCAACTG
Cd36	GGACATTGAGATTCTTTTCCTCTG	GCAAAGGCATTGGCTGGAAGAAC
Cntf	AGAGAGTGCATTTCACCCCG	TCTGTTCCAGAAGCGCCATT
CycA (HK)	GCGTCTCCTTCGAGCTGTT	AAGTCACCACCCTGGCA
Elovl1	TTGGCTGAGTACCTACACCTG	CTCGAACCATCCGAAGTGCTT
Elovl2	CACGTACCTGCTCTCGATATGG	TGTGATTGCGAGGTTATACAAGG
Elovl3	TTCTCACGCGGGTTAAAAATGG	GGCCAACAACGATGAGCAAC
Elovl4	GTCCTGAACGCGATGTCCA	GAGATAGAGCGTGCTTATGCTT
Elovl5	GAACATTTCGATGCGTCACTCA	GGAGGAACCATCCTTTGACTCTT
Elovl6	GAAAAGCAGTTCAACGAGAACG	AGATGCCGACCACCAAAGATA
Elovl7	CATCGAGGACTGTGCGTTTTT	GCCCAGGATGATGGTTTGTG
Hprt1 (HK)	CTCATGGACTGATTATGGACAGGAC	GCAGGTCAGCAAAGAACTTATAGCC
Igf1	TACTTCAACAAGCCCACAGGC	ATAGAGCGGGCTGCTTTTGT
Il1b	GAAATGCCACCTTTTGACAGT	TGGATGCTCTCATCAGCACA
Il6	TGTCTATACCACTTCACAAGTCGGAG	GCACAACTCTTTTCTCATTTCCAC
Nos2	GGCAGCCTGTGAGACCTTTG	GCATTGGAAGTGAAGCGTTTC
Lrp1	TCAGACGAGCCTCCAGACTGT	ACAGATGAAGGCAGGGTTGGT
Ngf	GGAGCGCATCGAGTTTTGG	TCCTTGGCAAAACCTTTATTGGG
Tbp (HK)	ATGGTGTGCACAGGAGCCAAG	TCATAGCTACTGAACTGCTG
Tgfb1	GGGCTACCATGCCAACTTCTG	GAGGGCAAGGACCTTGCTGTA
Tnfa	CCAGACCCTCACACTCAG	CACTTGGTGGTTTGCTACGAC

Abca1: ATP binding cassette subfamily A member 1, Abcg1: ATP binding cassette subfamily G member 1, Arg1: Arginase 1, Cntf: Ciliary neurotrophic factor, CycA: Cyclin A, Elovl: Elongation of very long-chain fatty acids proteins, HK: Housekeeping gene, Hprt1: Hypoxanthine phosphoribosyltransferase 1, Igf1: Insulin-like growth factor 1, Il: Interleukin, Nos2: Nitric oxide synthase 2, Lrp1: Low density lipoprotein receptor-related protein 1, Ngf: Nerve growth factor, Tbp: TATA-box binding protein, Tgfb1: Transforming growth factor beta 1, Tnfa: Tumor necrosis factor α.

Table S3 – List of antibodies

Antibody	Supplier, cat. number, concentration	Secondary antibody (Supplier, cat. number, concentration)	Use
7AAD	Thermo Fisher Scientific, 00-6993-50, 0.5 µg/ml	-	FACS
BODIPY 493/503	Thermo Fisher Scientific, D3922, 2 µM	-	FACS
Anti-ABCA1	Novus Biologicals, NB400-132, 1:400	Goat anti-rabbit Alexa Fluor 488 (Invitrogen, A11008, 1:300)	FACS
	Abcam, Ab18180, 1:500	Goat anti-mouse Alexa Fluor 555 (Invitrogen, A28180, 1:500)	ICC
Anti-MBP	Millipore, MAB386, 1:250	Goat anti-rabbit Alexa Fluor 488 (Invitrogen, A11008, 1:500)	IHC
Anti-NF	Abcam, Ab8135, 1:1000	Goat anti-rat Alexa Fluor 555 (Invitrogen, A21434, 1:500)	IHC
Anti-ELOVL1	Sigma, SAB4300768, 1:2000	Goat anti-rabbit Immunoglobulins/HRP (Dako, P0448, 1:5000)	WB

7AAD: 7-Aminoactinomycin D, ABCA1: ATP binding cassette subfamily A member 1, ELOVL: Elongation of very long-chain fatty acids proteins, FACS: Fluorescence-activated cell sorting, ICC: Immunocytochemistry, IHC: Immunohistochemistry, MBP: Myelin basic protein, NF: Neurofilament, WB: Western blot.

SUPPLEMENTARY RESULTS

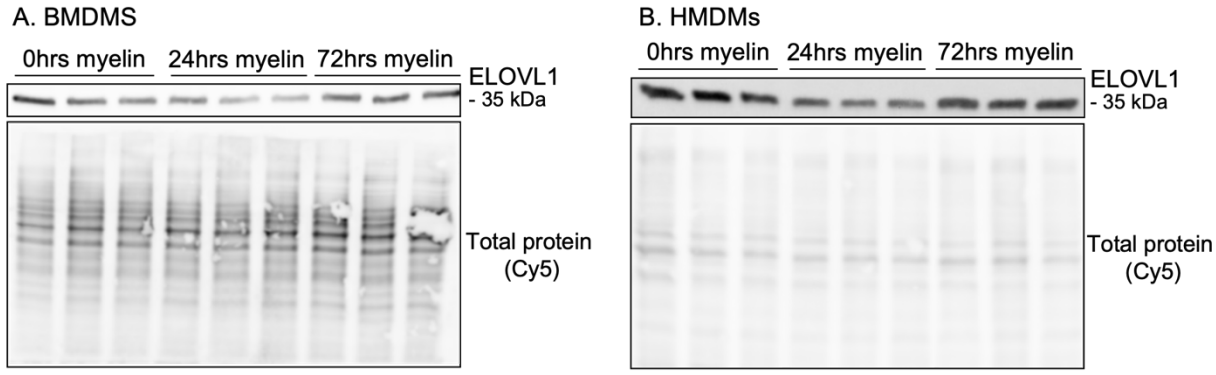

Fig. S1 – Representative images of western blot analysis of ELOVL1 in murine and human macrophages. (A) Murine bone marrow-derived macrophages (BMDMs) and (B) human monocyte-derived macrophages (HMDMs) that were left untreated (0 h) or treated with acute exposure (24 h) or with sustained exposure (72 h) to 100 μg/ml murine and 10 μg/ml human myelin, respectively (n = 3 wells). Protein abundance of ELOVL1 was normalized for total protein by Cy5.

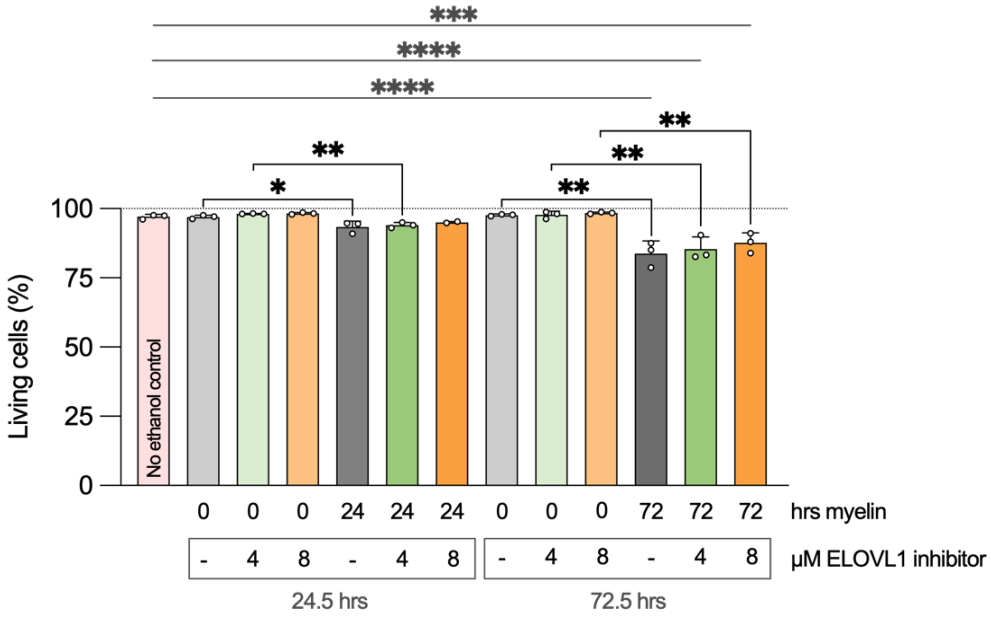

Fig. S2 – A concentration of 4 and 8 µM ELOVL1 inhibitor does not affect the viability of BMDMs. BMDMs were pre-treated with 4 or 8 µM ELOVL1 inhibitor or vehicle for 30 min and were subsequently exposed to myelin for 24 h or 72 h or left untreated. Cell viability was measured by 7AAD staining (n = 2-3 wells). A no-ethanol control was taken into account to assess the potential effects of ethanol. Data are represented as mean ± SD. *, $P < 0.05$; **, $P < 0.01$; ****, $P < 0.0001$; one-way ANOVA.

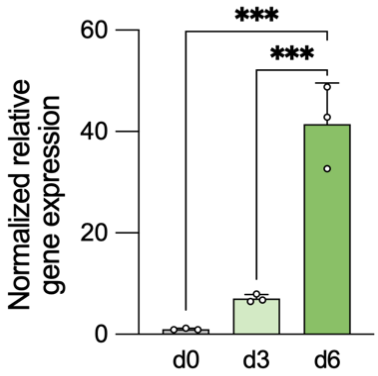

Fig. S3 – Validation of oligodendrocyte precursor cell (OPC) differentiation by myelin basic protein (Mbp) expression. Mbp expression was analyzed at day 0, 3, and 6 of OPC differentiation (n = 3 wells). High Mbp expression corresponds to mature oligodendrocytes. Data are represented as mean ± SD. ***, $P < 0.001$; one-way ANOVA.